

Original  
8/25/86  
U 86 0222  
COPY



# DEVELOPMENT OF THE CATHODE FALL IN A PLANAR DISCHARGE IN HELIUM

H. C. CHEN  
(NSWC)

A. V. PHELPS  
(JOINT INST. FOR LAB ASTROPHYSICS)

NSWC MP 86-222

PLASMA PHYSICS PUBLICATION NO. 86-1

JUNE 1986

Approved for public release; distribution is unlimited.



LIBRARY COPY

AUG 25 1986

NAVAL SURFACE  
WEAPONS CENTER LIBRARY

## NAVAL SURFACE WEAPONS CENTER

White Oak, Silver Spring, Maryland 20903-5000

200  
30

<b>Report Documentation Page</b>			Form Approved OMB No. 0704-0188	
<p>Public reporting burden for the collection of information is estimated to average 1 hour per response, including the time for reviewing instructions, searching existing data sources, gathering and maintaining the data needed, and completing and reviewing the collection of information. Send comments regarding this burden estimate or any other aspect of this collection of information, including suggestions for reducing this burden, to Washington Headquarters Services, Directorate for Information Operations and Reports, 1215 Jefferson Davis Highway, Suite 1204, Arlington VA 22202-4302. Respondents should be aware that notwithstanding any other provision of law, no person shall be subject to a penalty for failing to comply with a collection of information if it does not display a currently valid OMB control number.</p>				
1. REPORT DATE <b>JUN 1986</b>	2. REPORT TYPE	3. DATES COVERED <b>00-00-1986 to 00-00-1986</b>		
<b>4. TITLE AND SUBTITLE</b> <b>Development of the Cathode Fall in a Planar Discharge in Helium</b>			5a. CONTRACT NUMBER	
			5b. GRANT NUMBER	
			5c. PROGRAM ELEMENT NUMBER	
<b>6. AUTHOR(S)</b>			5d. PROJECT NUMBER	
			5e. TASK NUMBER	
			5f. WORK UNIT NUMBER	
<b>7. PERFORMING ORGANIZATION NAME(S) AND ADDRESS(ES)</b> <b>Naval Surface Weapons Center, White Oak, Silver Spring, MD, 20903-5000</b>			8. PERFORMING ORGANIZATION REPORT NUMBER	
<b>9. SPONSORING/MONITORING AGENCY NAME(S) AND ADDRESS(ES)</b>			10. SPONSOR/MONITOR'S ACRONYM(S)	
			11. SPONSOR/MONITOR'S REPORT NUMBER(S)	
<b>12. DISTRIBUTION/AVAILABILITY STATEMENT</b> <b>Approved for public release; distribution unlimited</b>				
<b>13. SUPPLEMENTARY NOTES</b>				
<b>14. ABSTRACT</b>				
<b>15. SUBJECT TERMS</b>				
<b>16. SECURITY CLASSIFICATION OF:</b>			<b>17. LIMITATION OF ABSTRACT</b> <b>Same as Report (SAR)</b>	<b>18. NUMBER OF PAGES</b> <b>37</b>
a. REPORT <b>unclassified</b>	b. ABSTRACT <b>unclassified</b>	c. THIS PAGE <b>unclassified</b>		

### Abstract

The time and spatial evolution of the cathode region of a planar discharge in helium has been modeled using numerical solutions of the electron and positive ion continuity equations and Poisson's equations. Single step ionization, electron and ion drift and diffusion, and electron-positive ion recombination are included using rate and transport coefficients based on experiment. The model is applied to high pressure, high current discharges such as found in electron-beam or photon initiated lasers. The cathode fall is found to approach steady-state voltage drop and sheath thickness are compared with experiment and previous theory using appropriate scaling laws.

## I. INTRODUCTION

The time and spatial evolution of ionization growth in planar discharge in helium has been studied using electron and positive ion rate equations, Poisson's equation, and experimental transport and rate coefficients. A numerical method is described for tracing theoretically the transient behavior of a rapidly developing gaseous discharge where the space-charge-distorted field is very important. We undertook this study of the cathode fall region as an initial step toward the solution of the growth of discharge instabilities in a three-dimensional geometry. In addition, there appear to be only very limited calculations<sup>1-3</sup> the time-dependent growth of this boundary layer. This paper presents numerical calculations of the quantities characteristic of cathode fall phenomena and a comparison of the numerical results with experiments and other theories. Section II describes the fundamental theory and numerical scheme used in our calculations. The results of the calculations are shown in Section III and are discussed in Section IV.

## II. THEORY

### A. Basic Equations

The planar discharges considered here are the discharges developed on an area with a diameter large compared with the gap length. They can be treated theoretically by a one-dimensional model. The electron and positive ion rate equations, Poisson's equation, and experimental transport and rate coefficients are used for tracing the growth in time and space of a one-dimensional helium discharge where the electric field is distorted by the space charge of the electrons and ions. The continuity equation for electrons is

$$\frac{\partial n_e}{\partial t} + \nabla \cdot (n_e \tilde{u}) = v n_e - \alpha n_e n_+ \quad (1)$$

where  $n_e$  and  $n_+$  are the electron and positive ion densities,  $t$  is the time,  $v$  is the ionization coefficient, and  $\alpha$  is the recombination coefficient. The electron velocity  $\tilde{u}$  can be expressed in terms of drift and diffusion velocity as

$$\tilde{u} = -\mu \tilde{E} - \frac{\nabla(n_e D)}{n_e} \quad (1a)$$

where  $\tilde{E}$  is the electric field,  $D$  and  $\mu$  are the diffusion and mobility coefficients of the electrons, respectively.

The continuity equation for positive ions is

$$\frac{\partial n_+}{\partial t} + \nabla \cdot (n_+ \tilde{u}_+) = v n_e - \alpha n_e n_+ \quad (2)$$

The ion velocity  $\tilde{u}_+$  can be expressed as

$$\tilde{u}_+ = \mu_+ E \quad (2a)$$

where  $\mu_+$  is the mobility of positive ions. The diffusion of the ions has been neglected because of their heavy mass. In these calculations, the ion drift flux is always greater than the ion diffusion flux by at least a factor of 100.

Poisson's equation describing the space-charge-distorted fields is

$$\frac{\partial E}{\partial z} = \frac{e}{\epsilon_0} (n_+ - n_e) \quad (3)$$

where  $e$  is the electronic charge,  $\epsilon_0$  is the permittivity of free space and  $z$  is the position in the axial direction.

The coefficients  $D$ ,  $v$ ,  $\alpha$ ,  $u_+$  and  $\mu$  must be taken from the experimental measurement or electron transport coefficient calculations. For atomic helium they are expressed in terms of the ratio of electric field to gas density  $E/N$  in the unit of  $V - cm^2$  and shown in Eq. (8) of Reference 4. Some of them have been modified because of the larger range of  $E/N$  throughout the discharge gap (i.e.  $10^{-18} V-cm^2 < E/N < 5 \times 10^{-15} V-cm^2$ ). Those used in the numerical calculations are listed for convenience as follows:

$$\mu N = 2.3 \times 10^{22} (cm-V-sec)^{-1}$$

$$\mu_+ N = 2.9 \times 10^{20} (300/T_N)^{0.26} (cm-V-sec)^{-1}$$

$$\alpha = [1.13 \times 10^{-8} + 4.22 \times 10^{-29} N T_N] 300/T(0k) cm^3 sec^{-1} \quad (4)$$

$$v/N = 4.6 \times 10^5 (E/N) (1 + 5 \times 10^{14} E/N) \exp(-7 \times 10^{-16} N/E) \text{ cm}^3 \text{ sec}^{-1}$$

$$D = \mu k T/e$$

where

$$T = 300 + 3 \times 10^{20} (E/N) / \left\{ 1 + [5 \times 10^{10} (E/N)^{2/3}]^6 \right\}^{1/6}.$$

Here D is the longitudinal diffusion coefficient, k is the Boltzmann constant and  $T_N$  is the gas temperature in Kelvin.

An allowance has been made for the time required for electrons emitted from the cathode to attain the ionization rate appropriate to the local E/N value by requiring the electrons to pass through a potential of 40 V before ionization begins. This approximation is an extension of the observations for a uniform electric field<sup>5</sup> to the present spatially varying electric field. In practice, the following smooth function has been used for the ionization rate coefficient.

$$f = \begin{cases} \frac{1}{2} \left( \frac{V}{40} \right)^{10} & \text{for } 0 < V < 40 \\ 1 - \frac{1}{2} \left( \frac{80-V}{40} \right)^{10} & \text{for } 40 < V < 80 \end{cases} .$$

## B. Boundary Conditions

At the cathode, secondary electrons are produced by the bombardment of ions and photons

$$\Gamma_e(0) = \gamma_+ \Gamma_+(0) + \gamma_p \Gamma_p, \quad (5)$$

where  $\Gamma_i$  represents the flux of various particles i.  $\gamma_+$  and  $\gamma_p$  are the secondary coefficients representing the probability of the production of secondary electrons at the cathode per incident positive ion or photon. The effect of photons is to enhance the production of secondary electrons and speed up the formation of the cathode fall at the early times in discharge which will be demonstrated in Section III.B.

At the anode, we have zero density for both electrons and ions

$$n_e(d) = n_+(d) = 0 \quad . \quad (6)$$

where  $d$  is the distance between two electrodes. The voltage across the discharge gap is  $V$  so that the boundary condition for Eq. (3) is

$$\int_0^d E dz = V. \quad (7)$$

Equation (1) is a second order partial differential equation with two boundary conditions. Equations (2) and (3) are first order partial differential equations with one boundary condition. Therefore, we have a complete set of three partial differential equations that can be solved numerically for the three unknown  $n_e$ ,  $n_+$  and  $E$ . Note that the boundary condition in Eq. (5) is a combination of Neumann and Dirichlet boundary condition which has the form  $A n + B (\partial n / \partial z) = C$  where  $A$ ,  $B$  and  $C$  are constant. An imaginary point outside the boundary has to be introduced in the finite difference frame. For ion equation, we can use one-sided difference approximation for the cathode boundary.

### C. Current Continuity and External Circuit

The large potential drop between the cathode and the negative glow is normally called the cathode fall. It is one of the most important quantities describing the glow discharge. In order to obtain relations between the cathode fall  $V_c$ , current density  $J$  and thickness of the cathode fall  $d_c$  and compare the calculated quantities to the experimental measurements, an external circuit with a constant external resistance  $\Omega$  and a constant voltage source  $V_0$  have been added in the discharge problem. The effects of circuit inductance and capacitance has been neglected so that we have the simple circuit equation

$$V_0 = V + J\Omega A, \quad (8)$$

where  $J$  represents the total ionization current density which can be calculated by the following energy balance method.

The power fed by the voltage supply  $V$  across the discharge gap is equal to the sum of the power delivered to the gas and the rate of change in electrostatic energy, i.e.,

$$JV = \int_0^d \vec{E} \cdot \vec{J} dz + \frac{\partial}{\partial t} \int_0^d \frac{\epsilon_0 E^2}{2} dz. \quad (9)$$

Equation (9) can be further simplified for constant  $V$  by using Green's theorem as<sup>6</sup>

$$Jd = e \int_0^d (n_e u + n_+ u_+) dz. \quad (10)$$

It will be noticed that Eq. (10) relates the energy input to the gap to the integral of the energy dissipated per unit volume and include changes in the energy stored in the electric field, i.e., the displacement current. In the numerical calculations, for each time step we use Eq.(10) to calculate  $J$  first and then use Eq. (8) to adjust  $V$  to insure consistency of  $V$  with the assumed  $V_0$  and  $\Omega A$ . The value of  $1 \text{ cm}^2$  for  $\Omega A$  has been used in the calculations throughout the paper exclusively.

#### D. Numerical Scheme

A Crank-Nicholson finite difference scheme<sup>7</sup> which is implicit both in time and space has been used and a predictor-corrector step has been added to take into account the nonlinear coefficients in the equations. Use of nonuniform spatial step-sizes has been found very effective in studying the time development of the boundary layer in the cathode fall region. Equations (1) to (3) can be generalized by the following equation

$$\frac{\partial n}{\partial t} = \beta n + n \frac{\partial n}{\partial z} + \gamma \frac{\partial^2 n}{\partial z^2} + \xi , \quad (11)$$

where  $\beta$ ,  $n$ ,  $\gamma$  and  $\xi$  may be functions of  $z$  and  $n$ .

Using Taylor series expansion or Lagrange interpolation formula, the first and second spatial derivatives can be approximated by a centered difference in space as

$$\frac{dn}{dz} = A_1 n_{j-1} + B_1 n_j + C_1 n_{j+1} ,$$

and

$$\frac{d^2n}{dz^2} = A_2 n_{j-1} + B_2 n_j + C_2 n_{j+1} .$$

The Crank-Nicholson scheme yields for the general Eq. (11)

$$\frac{n_j^{t+1} - n_j^t}{\Delta t} = \xi_j^t + \beta_j \frac{n_j^{t+1} + n_j^t}{2} + \eta_j^t \delta_x \frac{n_j^{t+1} + n_j^t}{2} + \gamma_j^t \delta_{xx} \frac{n_j^{t+1} + n_j^t}{2} , \quad (12)$$

where we use the operator notation

$$\delta_x n^t = A_1 n_{j-1}^t + B_1 n_j^t + C_1 n_{j+1}^t$$

$$\delta_{xx} n^t = A_2 n_{j-1}^t + B_2 n_j^t + C_2 n_{j+1}^t .$$

Equation (12) along with boundary conditions [Eqs. (5) to (7)] can be solved for each unknown by inverting a tridiagonal matrix.

In order to have the scheme completely implicit and stable, the coefficients  $\beta$ ,  $\eta$ ,  $\gamma$ ,  $\xi$  have to be centered in time. We then use a predictor-corrector iterative scheme with

$$\begin{aligned} \frac{\hat{n}_j^{v+1} - n_j^t}{\Delta t} &= \hat{\xi}^{v+1/2} + \hat{\beta}^{v+1/2} \frac{\hat{n}_j^{v+1} + n_j^t}{2} + \hat{\eta}^{v+1/2} \delta_x \frac{\hat{n}_j^{v+1} + n_j^t}{2} \\ &+ \hat{\gamma}^{v+1/2} \delta_{xx} \frac{\hat{n}_j^{v+1} + n_j^t}{2} , \end{aligned}$$

$$\hat{n}_j^0 = n_j^t ,$$

and

$$n_j^{t+1} = \hat{n}_j^p .$$

We could iterate to convergence by choosing the number of iterations  $p$  at each time step so that

$$\max_j \left| \hat{n}_j^p - \hat{n}_j^{p-1} \right| < \epsilon .$$

For suitable  $\epsilon$ , we could stop the iteration and set  $n_j^{t+1} = \hat{n}_j^p$ . Usually a stable scheme takes no more than two iterations for each time step.

As discussed in Appendix A the diffusion term in Eq. (1) is very important in the calculation in conjunction with the numerical instabilities. The expression for  $D$  in Eq. (4) has been chosen carefully for the best fit to the experimental observations. Experience suggests that in order to solve the set of Equations (1) to (3) without numerical instability we have to modify Eq. (1a) as

$$u = - \mu E - D \frac{\nabla n_e}{n_e} \quad (13)$$

where the diffusion coefficient  $D$  has been outside of the gradient. Eq. (13) has been used throughout the paper exclusively. Furthermore, in the time evolution of the cathode fall, the electron equation becomes very stiff in the early time around 0.07  $\mu$ sec for the case run without introducing the external circuit. Because of this, the set of partial differential equations [Eqs. (1) to (3)] has been solved with the diffusion term [second order term in Eq. (1)] increased by a factor of 2. The enhanced diffusion term is used to damp<sup>7</sup> the high frequency terms in the solution without affecting the desired solution too much (see Appendix A).

### III. NUMERICAL RESULTS

#### A. Initial Conditions

A stable difference scheme is not unduly sensitive to small perturbations so that an initial condition can be chosen arbitrarily. As in a double discharge laser the discharges considered here are initiated by an electron and ion pair whose density varies smoothly along  $z$  and has a peak value of  $3 \times 10^{10} \text{ cm}^{-3}$ . This initial ionization with Lorentz profile as shown in Figure 1 has the following simple relation with  $z$

$$n(z,0) = 3 \times 10^{10} [1 + (z/d - 0.5)^2]^{-16} \text{ cm}^{-3}. \quad (14)$$

An alternate initial condition is

$$n(z,0) = 1.2 \times 10^{11} (z/d) (1 - z/d) \text{ cm}^{-3}. \quad (15)$$

Where the same value of  $3 \times 10^{10} \text{ cm}^{-3}$  was chosen at the center of the gap in Eqs. (14) and (15). Calculations are shown for a gap length of 2 cm, a helium density  $N$  of  $3 \times 10^{19} \text{ cm}^{-3}$ , temperature  $T_N$  of 300°K, and initial  $E/N$  of  $1.8 \times 10^{-16} \text{ V-cm}^2$ . A  $\gamma_+$  of 0.09 has been chosen and the effect of photons has been neglected in the calculations shown except in Figure 7. It is known that the quantities characteristic of cathode fall phenomena do not depend on the length of the discharge. The effect of gas heating is neglected at this stage so that  $T_N$  and  $N$  are assumed independent of time and space.

Figure 2 shows that the electric field is reduced by charge separation in the region of maximum initial ionization at the very earlay time (e.g., 0.02  $\mu\text{sec}$ ). The density difference between electrons and ions is very small

in the plasma region. The field near cathode increases as the electrons are swept toward the anode. The significant ionization occurs due to the increase of electric field in the cathode sheath. This large source of ionization causes a remarkable increase in the positive ion density while the electrons are moving away from the cathode sheath continuously. The field increases near the cathode until it becomes high enough to cause an ionization wave to move toward the cathode.<sup>8</sup> This is illustrated in Figure 3 for two different times. Note that the figures show only the small region within 0.03 cm of the cathode. The electric field near cathode becomes high and forms the cathode fall. At  $t = 0.12 \mu\text{sec}$ , as shown in Figure 4, the current density is  $3.4 \text{ amperes/cm}^2$  and the thickness of cathode fall is about  $2.4 \times 10^{-3} \text{ cm}$ . It is noted that Figures 2 to 4 show results obtained using initial profile (Eq. (14)) and boundary condition (Eq. (7)) with constant V. As mentioned early the diffusion coefficient D has been enhanced by a factor of 2. The sequence of electric field and charge distributions in the cathode fall region is essentially independent of gap length with the time scale decreasing from  $\sim 200 \text{ ns}$  for a 3 mm gap and 100% overvoltage to  $\sim 60 \text{ ns}$  for a 7 cm gap and 50% overvoltage.

In order to compare our results with other theories, the circuit equation (8) has been added in the calculations from this point on. Figure 5 shows the transient behavior of the discharges with  $\Omega A = 1 \text{ ohm} - \text{m}^2$  for initial condition (Eq. (15)). The similar results for initial condition (Eq. (14)) except in the very early time suggests that we can choose any arbitrary initial conditions. The distributions of electric field, electron and ion densities change drastically prior to  $0.1 \mu\text{sec}$  due to the propagation of the ionization wave. It then takes a rather longer time to reach the steady-state solution as shown at  $t = 0.4 \mu\text{sec}$ . We see little difference between the curves at  $0.3 \mu\text{sec}$  and at  $t = 0.4 \mu\text{sec}$ . Following convention, the cathode fall distance

and cathode fall voltage are determined by extending the straight line portion of the electric field to the point where the electric field is zero. This is illustrated in Figure 6 which shows the values of  $J_e$ ,  $J_i$ ,  $E$ , and  $J$  of Figure 5 at  $t = 0.4 \mu\text{sec}$  as a function of the distance from the cathode. Note that  $J = J_e + J_i$  is the total current density and is independent of the distance from the cathode.

At the cathode there are few electrons and the current is carried mainly by ions; in the negative glow region where the field is very small, the ion and electron numbers are more equal but because of their greater mobility the electrons carry the current. Experimentally field measurements are used to define  $d_c$  as the point where the extrapolated field becomes zero<sup>9</sup> and then determine  $V_c$ . While none of the theories has yet been able to account for the experimentally observed linear change of field<sup>10</sup> in the cathode fall region, the calculations presented here have shown the linear decrease in field from cathode to the edge of the glow.

#### B. Effect of Electron Reflection of Cathode

In this subsection we examine the sensitivity of the solution to the boundary condition of the cathode. The Milne boundary condition<sup>11</sup> with the inclusion of cathode injection and electric field can be expressed as

$$n_e \frac{\bar{v}_e}{4} (1 - r) - \gamma n_+ \mu_+ E = D \frac{dn_e}{dz} - n_e \mu E , \quad (16)$$

where the electron mean velocity  $\bar{v}_e = (2 kT/m)^{1/2}$ ,  $r$  is the electron reflection coefficient and  $\gamma$  is the secondary coefficient from cathode. The left-hand side of Eq. (16) is the net flux of electrons arriving at the cathode from an imaginary boundary one mean-free-path into the gas, while the

right-hand side is the same flux as given by the usual transport coefficient formulation.

We choose  $r = 0.2$  and  $\gamma = 0.3$  and do the similar calculations as in A with new boundary conditions. The results shown in Figure 7 are very similar to Figure 5. Two different boundary conditions do not give any significant difference in the time evolution of the cathode fall region. The small difference for the electric field in the cathode sheath is due to the difference in the secondary coefficient  $\gamma$ . Note that  $\gamma$  is defined differently in both cases. Fig. 8 shows the growth of the electron and ion current density as well as the voltage drop through the gap. We can see the current has been saturated and reached the steady state for the case with external circuit. The difference of current density and voltage drop in the early time is due to a different choice of initial condition. A 140 Volt cathode fall was found at  $t = 0.4 \mu\text{sec}$ .

### C. Role of Metastables and Resonance Radiation

The rate equations for helium triplet ( $2^3S$ ) metastables T and singlet ( $2^1S$ ) metastables S are<sup>12</sup>

$$\frac{\partial T}{\partial t} = k_{eT} n_e N + \frac{D_T}{N} \frac{\partial^2 T}{\partial z^2} - k_{T3} N^2 T , \quad (17)$$

and

$$\frac{\partial S}{\partial t} = k_{es} n_e N + \frac{D_S}{N} \frac{\partial^2 S}{\partial z^2} - k_{S2} N S - k_{S3} N^2 S , \quad (18)$$

where  $k_{er}$  is the rate coefficient for excitation of species y at unit gas density,  $k_{y3}$  is three-body collision frequency for conversion species y into

metastable molecules,  $k_{y2}$  is two-body collisional frequency for species  $y$ ,  $D_y$  is the diffusion coefficient at unit gas density for species  $y$ . The current density of metastable atoms reaching the cathode by diffusion can be neglected on our short time scale. Also, since the metastable molecules do not radiate they do not produce a photocurrent.

Now the  $K_{S2}$  term in Eq. (18) is collision induced radiation so that the current of photons arriving at the cathode is

$$I_s = \frac{k_{S2}}{2} \int_0^d S dz . \quad (19)$$

Note that  $I_s$  includes the fraction (1/2) of nonresonance photons produced in the gap which are directed toward the cathode.

The differential equation governing the density of resonance radiation can be written as follows<sup>12</sup>

$$\begin{aligned} \frac{\partial R}{\partial t} = & k_{eR} n_e N - k_{R1} N R - k_{R2} N^2 R - k_{R0} R \\ & - A R + A \int_0^d R(z', t) K(|z-z'|) dz' , \end{aligned} \quad (20)$$

where  $A$  is radiative transition probability for the resonance transition,  $k_{eR}$  and  $K_{R0}$  are frequencies of excitation at unit gas density,  $K_{R1}$  and  $K_{R2}$  are two-body and three-body collision frequency respectively,  $K(|z-z'|)$  is transmission function for resonance radiation. The integral of  $K(|z-z'|)$  gives the probability that the resonance photons emitted at  $z$  will be absorbed at a point to the left of  $z = 0$  in the absence of the cathode or the probability the resonance photons will travel as far as the cathode before absorption.

If we use the Biberman approximation,<sup>12</sup> then

$$R - \int_0^d R(z', t) K(|z-z'|) dz' = R[G(z) + G(d-z)].$$

We use the approximation  $G(z) = 1/[16 + 81 (\pi k_p z)^2]^{1/4}$ , where  $k_p = 3\pi/\lambda_0$  and  $\lambda_0$  is the wavelength of the resonance line. The current of photons  $r_R$  becomes

$$\begin{aligned} r_R &= A \int_0^d R(z, t) dz \int_{-\infty}^0 K(|z-z'|) dz' \\ &= A \int_0^d R(z, t) dz \int_z^{\infty} K(y) dy \\ &= A \int_0^d R(z, t) G(z) dz . \end{aligned} \tag{21}$$

Both  $r_s$  and  $r_R$  contribute to  $r_p$  in Eq. (5). The coefficients used come from Table II and Fig. 3 of Reference 12 are listed below.

$$k_{es} = 2.8 \times 10^5 E \left(1 - \frac{E/N}{9 \times 10^{-16}}\right) \exp(-3.7 \times 10^{16} N/E) \text{ sec}^{-1}$$

$$k_{s2} = 6 \times 10^{-15} \text{ sec}^{-1}$$

$$k_{s3} < 10^{-32} \text{ sec}^{-1}$$

$$K_{eR} = 1.38 \times 10^5 E \exp(-3.8 \times 10^{-16} N/E) \text{ sec}^{-1}$$

$$k_{R1} = 2 \times 10^{-12} \text{ cm}^3 \text{ sec}^{-1}$$

$$k_{R2} = 9 \times 10^{-32} \text{ cm}^6 \text{ sec}^{-1}$$

$$k_{R0} = 1.9 \times 10^6 \text{ sec}^{-1}$$

$$\lambda_0 = 5.84 \times 10^{-6} \text{ cm}$$

$$A = 1.8 \times 10^9 \text{ sec} . \quad (22)$$

We next perform calculations similar to those in section III.A, i.e., with initial condition (Eq. (14)) and boundary condition (Eq. (5)). A  $\gamma_p$  of 0.05 has been chosen. The results are shown in Figure 9 and should be compared to Figure 5 in order to see the effect of photons on the evolution for the cathode fall. As pointed out previously, the time scale for the formation of the cathode fall has been shortened because of increased production of secondary electrons at the cathode at early times. Other than that, the effect of photons can hardly be seen in the later stage of the discharge because the ion term becomes dominant. A cathode fall of 183 Volt was found at 0.4  $\mu\text{sec}$  for the conditions of both Figure 5 and Figure 9.

#### IV. DISCUSSION

Although the mean free path for electrons with an average energy of  $\sim 5$  eV is small compared to the cathode sheath, a number of authors<sup>13</sup> have questioned the applicability of the continuum model implicit in Eqs. (1) and (2). As a partial answer to this question we calculate the energy relaxation distance<sup>14</sup> for conditions corresponding to those of Figure 4. The energy relaxation distance for the plasma region is about  $4 \times 10^{-5}$  cm which is very small compared to the dimension of the plasma region. A relaxation distance of  $3 \times 10^{-5}$  cm is found at the midpoint of the cathode fall region. Since the electric field varies by only 4% over this distance, we believe that the continuity equations are reasonably accurate.

Theoretically and experimentally numerous studies of the cathode fall region have been made to explain the mechanism of the cathode phenomena of the glow discharge. Various theories have been derived from a selection of the aforementioned fundamental equations, i.e., equations (1) to (3); most people use Townsend's  $\alpha$  for the rate of ionization and make different assumption about  $u_+$  and  $\alpha$  as a function of local electric field. For example, Von Engel and Steenbeck<sup>10</sup> omitted continuity equation and used instead the experimentally determined distribution of the field in the cathode fall region. Similar calculations have been made by Ward<sup>1</sup> except that he had to use different form for  $\alpha$  and  $u_+$  in order to get good agreement with experimental data. Experimentally,  $V_C$  has been defined and measured in a number of ways. The definition of  $V_C$  depends strictly upon the method used to measure it. Each method has certain inherent errors. Many experimenters have obtained results not agreeing with each other, and often not consistent and reproducible in their own apparatus. However, extensive cathode fall measurements have been made by Guntherschulze and co-workers.<sup>15</sup> In order to

eliminate the heating effect, they used in his measurements a very large massive cathode and low gas pressures.<sup>16</sup> Warren<sup>10</sup> has developed a refined electron beam technique to measure the field in the cathode-fall region. They all show an almost linear decrease of field to zero with distance from the cathode. No negative fields were found in the negative glow. He further pointed out that there are two theories of the cathode region which give results not agreeing well with experiment. One which assumes that ions moves across the cathode fall region freely (free fall theory); the other which assumes that ion has a drift velocity  $u_+$  proportional to the square root of electric field. All of their results for the cathode fall versus current density have been shown in Figure 10 where we have compared our results for the steady state for cathode fall.<sup>17</sup> We see that the calculated cathode fall voltage drop is close to steady-state values measured at much lower gas densities. Note that the cathode fall is a strong function of secondary coefficient  $\gamma$ .

Essentially the factor which determines  $V_C$  is  $\gamma$  which depends on the size and energy of the ions and photons hitting the cathode, on the cathode material and the state of its surface, and on the nature and pressure of the gas. The calculations have been made with an external resistance and fixed voltage supply so as to simulate experiments more accurately. Other processes which should be included in the model include the production, destruction and ionization of metastable atoms and molecules and the heating and motion of the neutral gas.<sup>18</sup> Obviously, further work is necessary to clarify the relationships among the various theoretical approaches to the cathode fall. At present, both the continuum model and the nearly free fall approaches seem to be able to use their methods to show their validity.

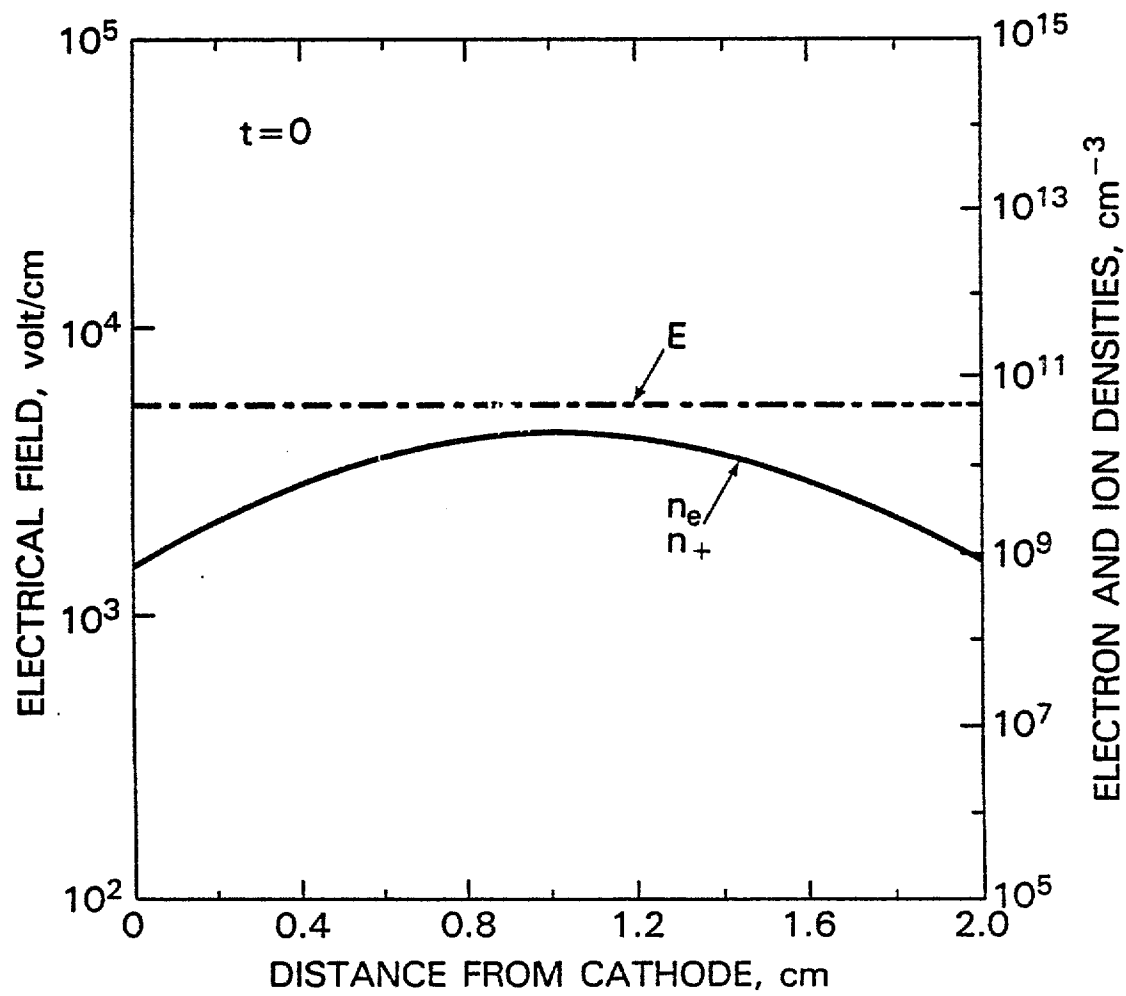


FIGURE 1. INITIAL DENSITIES OF ELECTRON AND ION AND ELECTRIC FIELD IN PARALLEL PLANE GAP

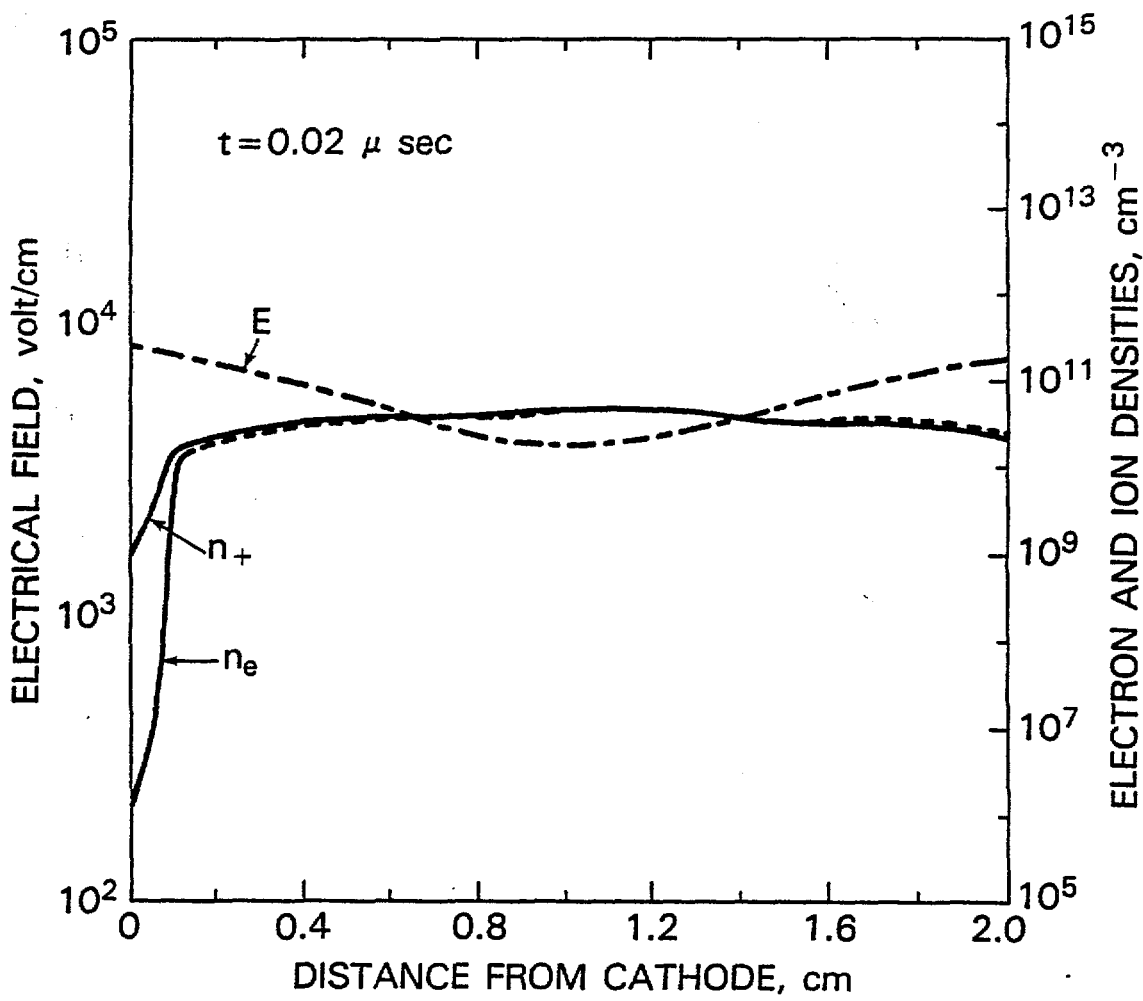


FIGURE 2. CALCULATED ELECTRON AND ION DENSITIES AND ELECTRIC FIELD AT  
 $t = .02 \mu\text{sec}$

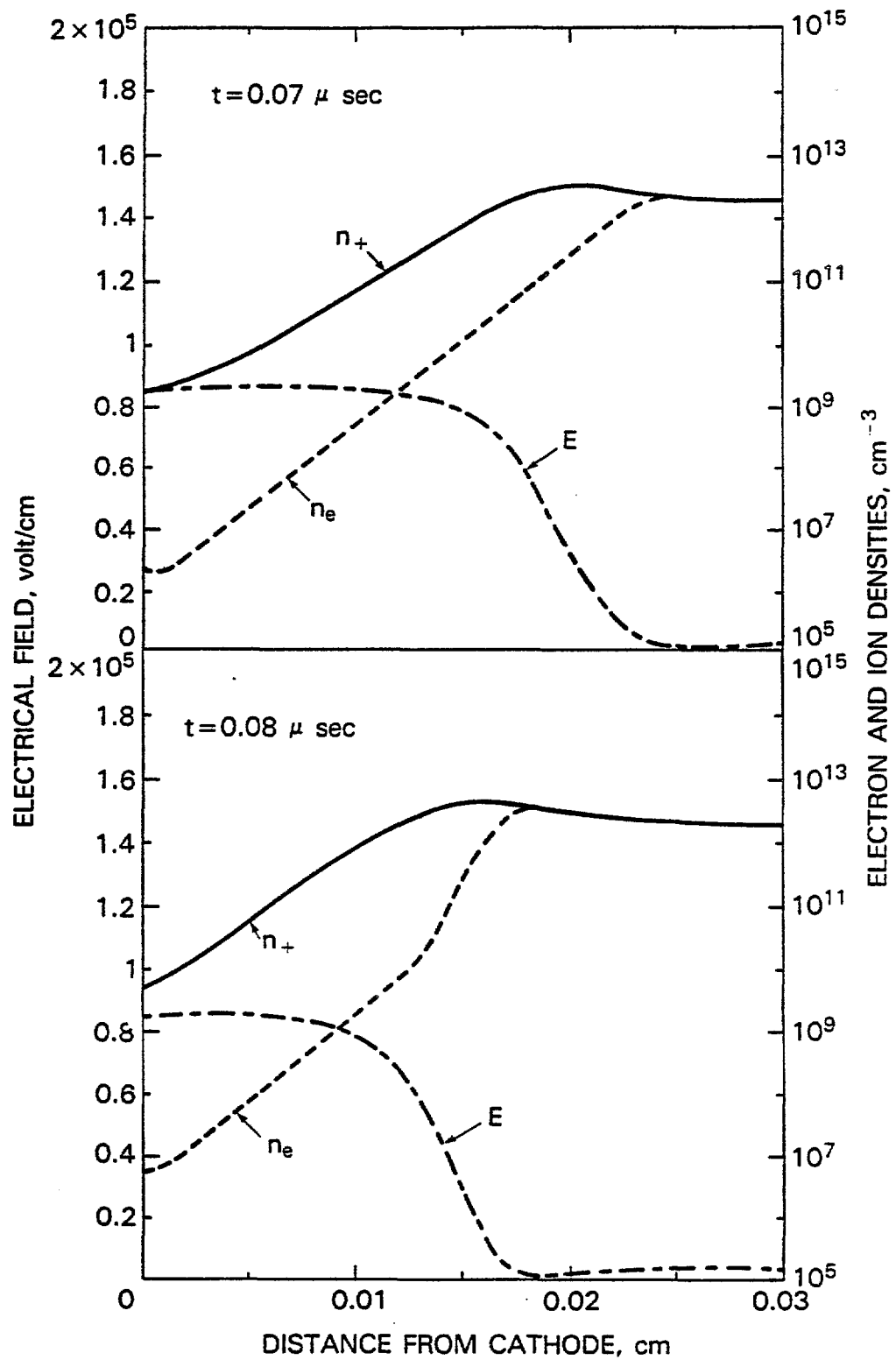


FIGURE 3. PROPAGATION OF THE IONIZATION WAVE: CALCULATED CHARGE DENSITIES AND ELECTRIC FIELD AT  $t = .07 \mu\text{sec}$  AND  $t = .08 \mu\text{sec}$

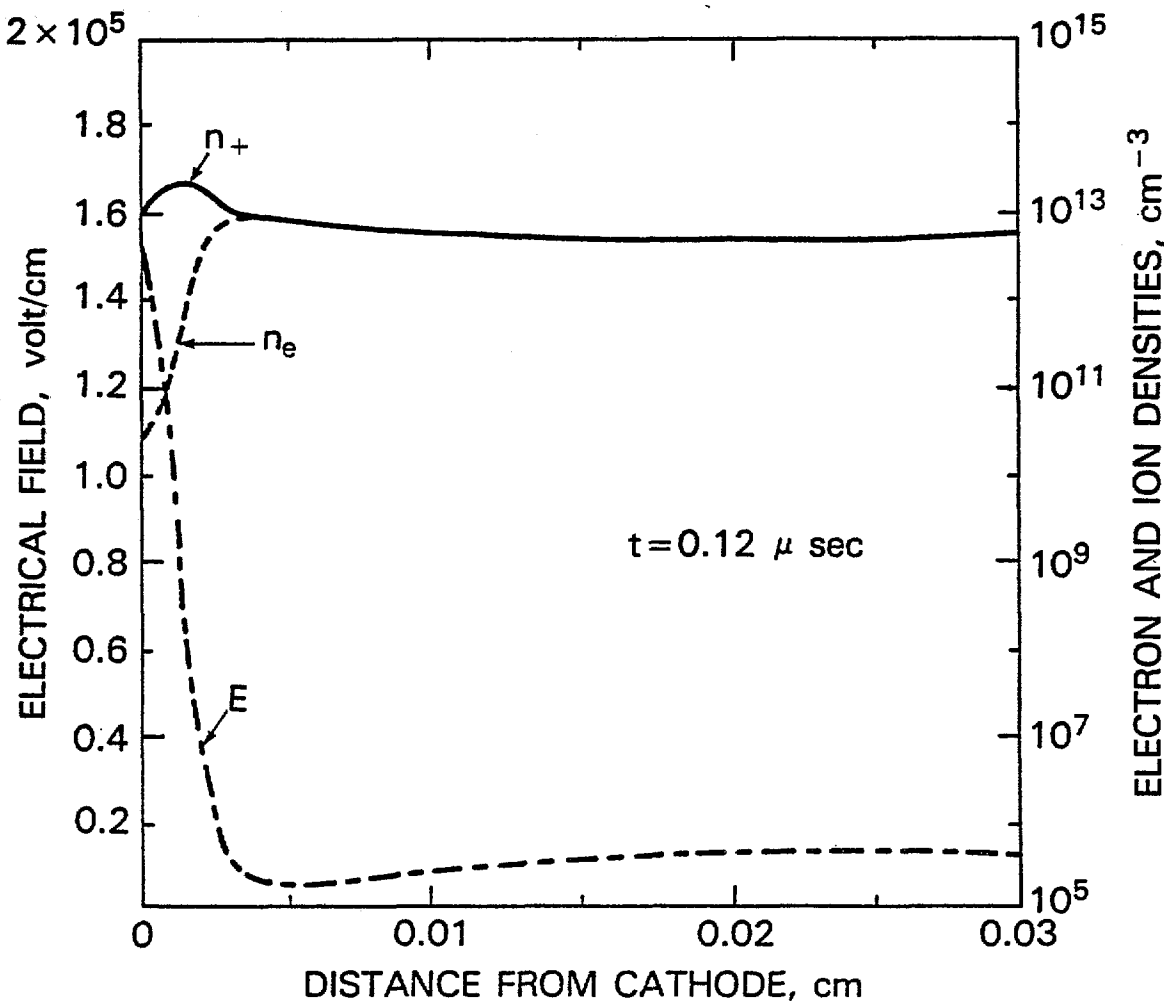


FIGURE 4. CALCULATED ELECTRON AND ION DENSITIES AND ELECTRIC FIELD NEAR CATHODE AT  $t = .13 \mu\text{sec}$ . THE CURRENT DENSITY IS  $10 \text{ AMPERE}/\text{CM}^2$

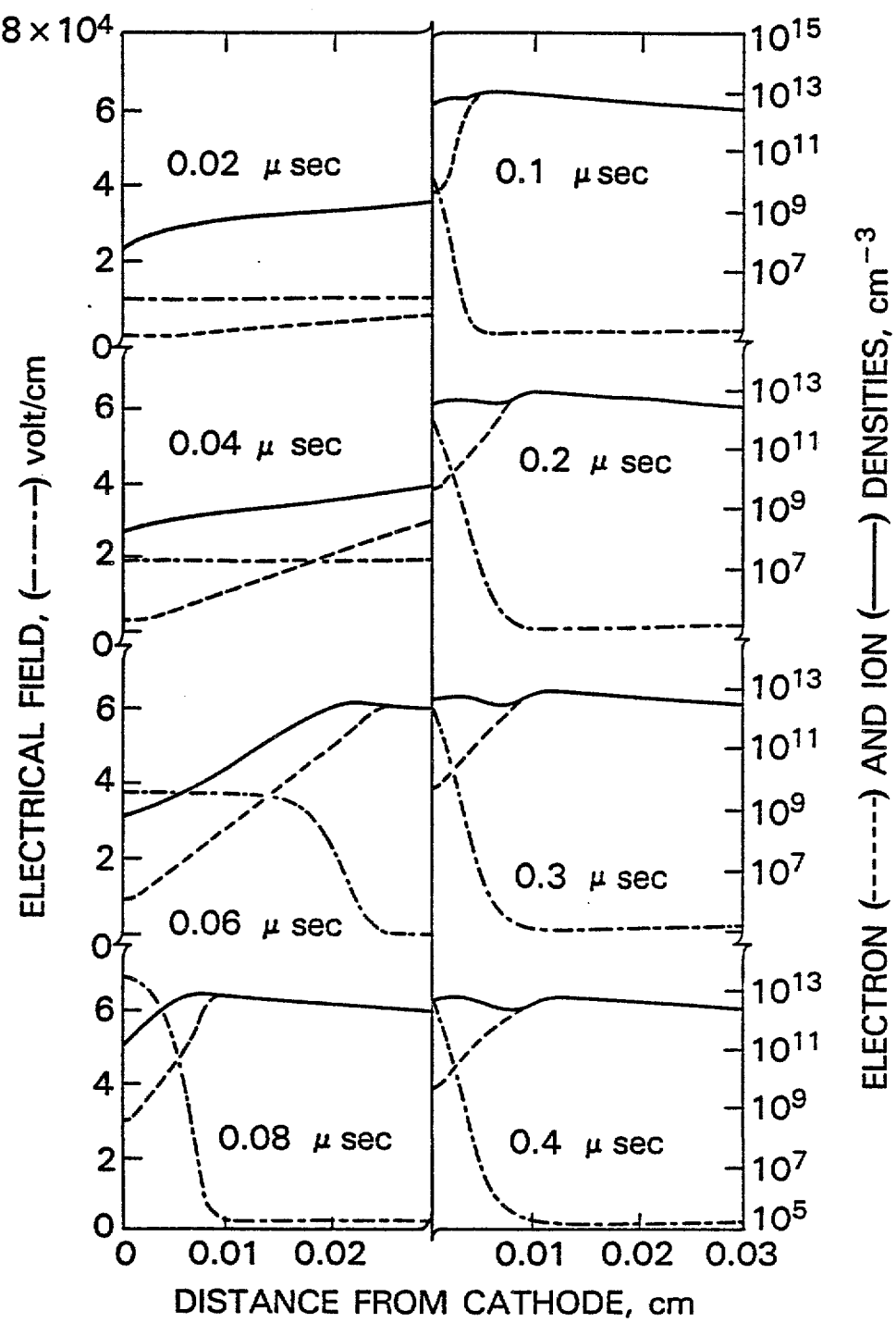


FIGURE 5. THE EVOLUTION OF THE CATHODE FALL REGION WITH INITIAL CONDITION (EQ. (15)) AND  $\Omega A = 1$  OHM-M<sup>2</sup>

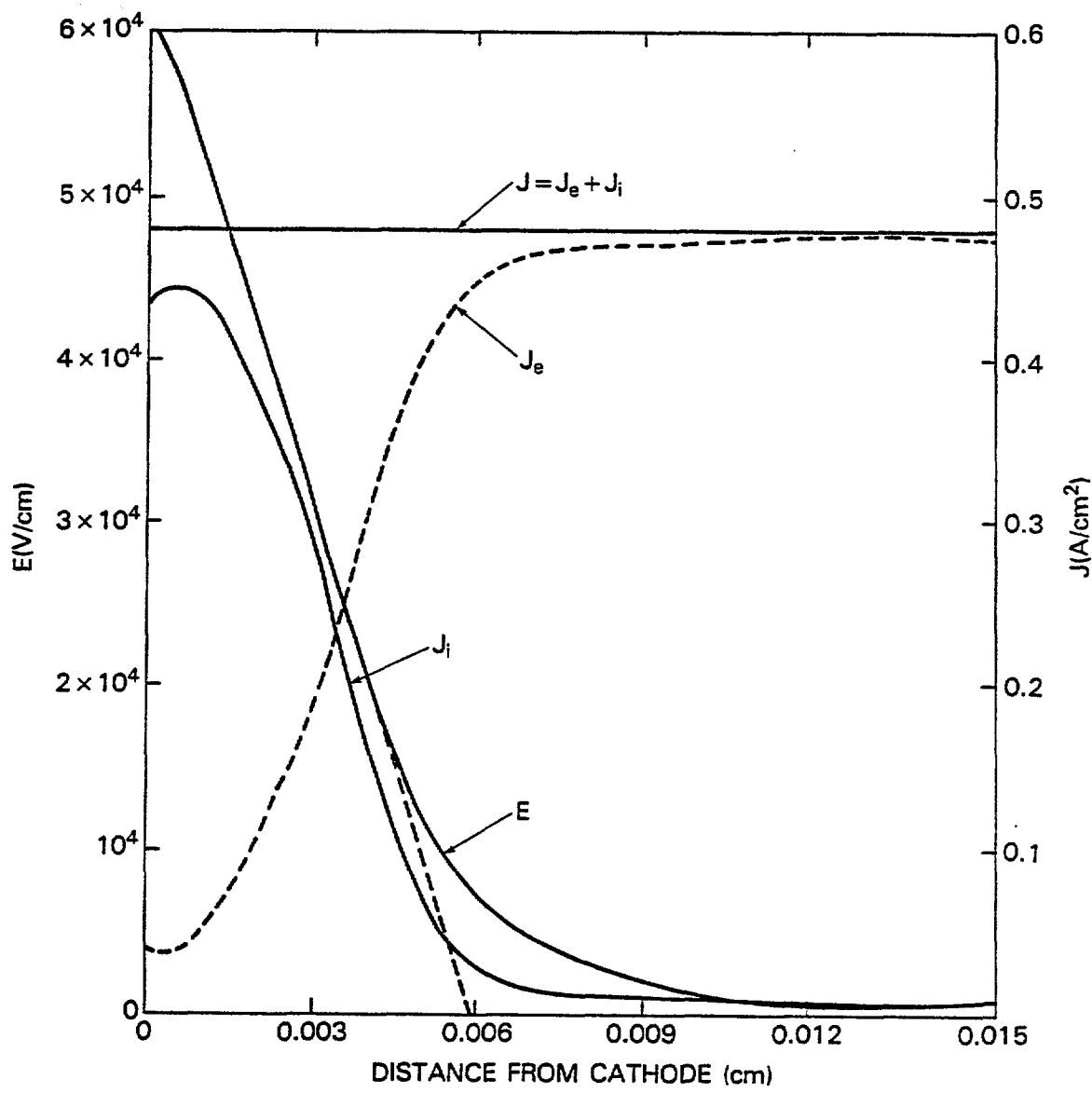


FIGURE 6. THE VALUES OF  $J_e$ ,  $J_i$ ,  $E$ , and  $J$  OF FIGURE 5 AT  $t = 0.4 \mu\text{sec}$  VERSUS DISTANCE FROM THE CATHODE

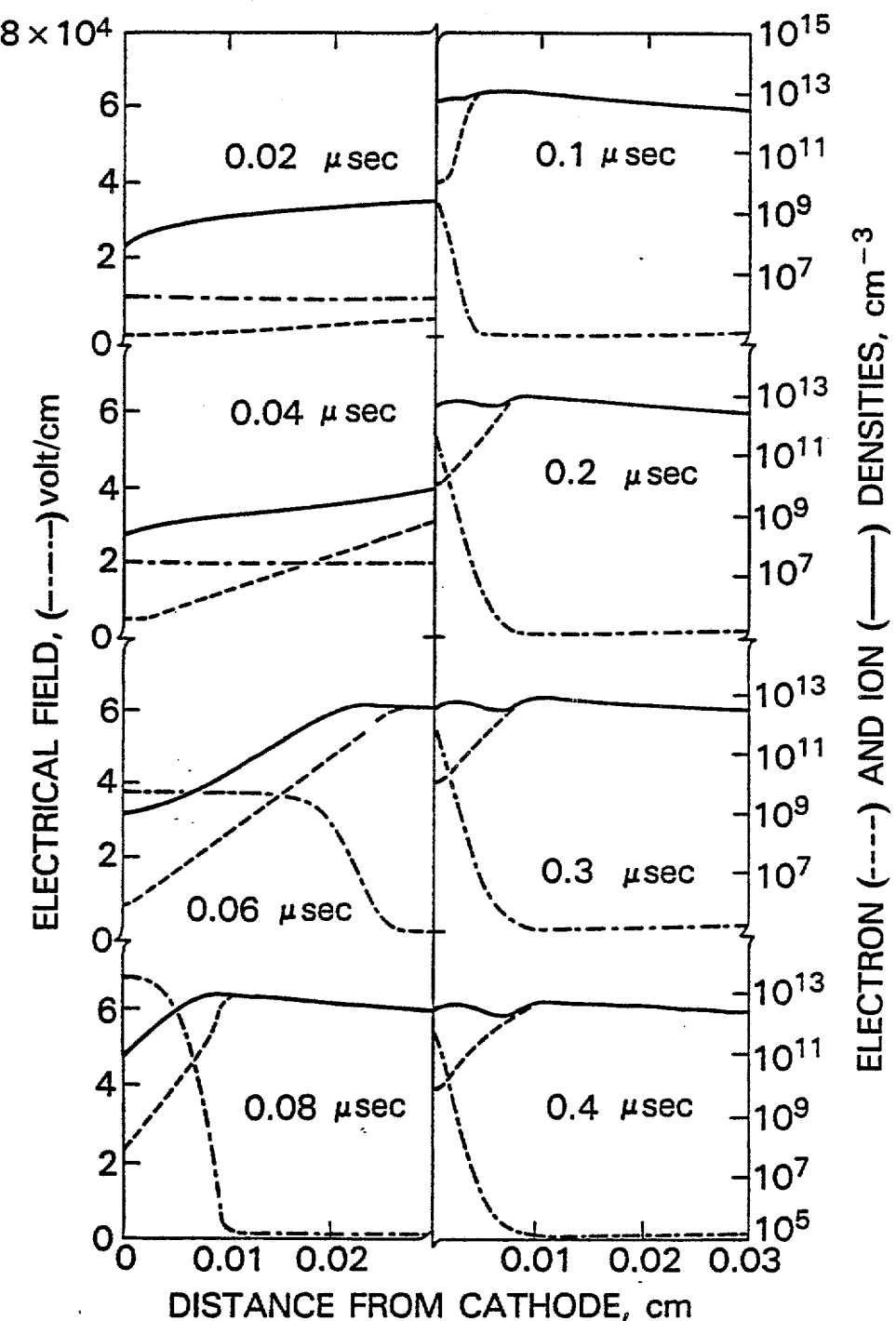


FIGURE 7. CALCULATIONS SIMILAR TO FIGURE 5 EXCEPT USING THE NEW BOUNDARY CONDITION (EQ. (16)) WITH  $r = 0.2$  and  $\gamma = 0.3$

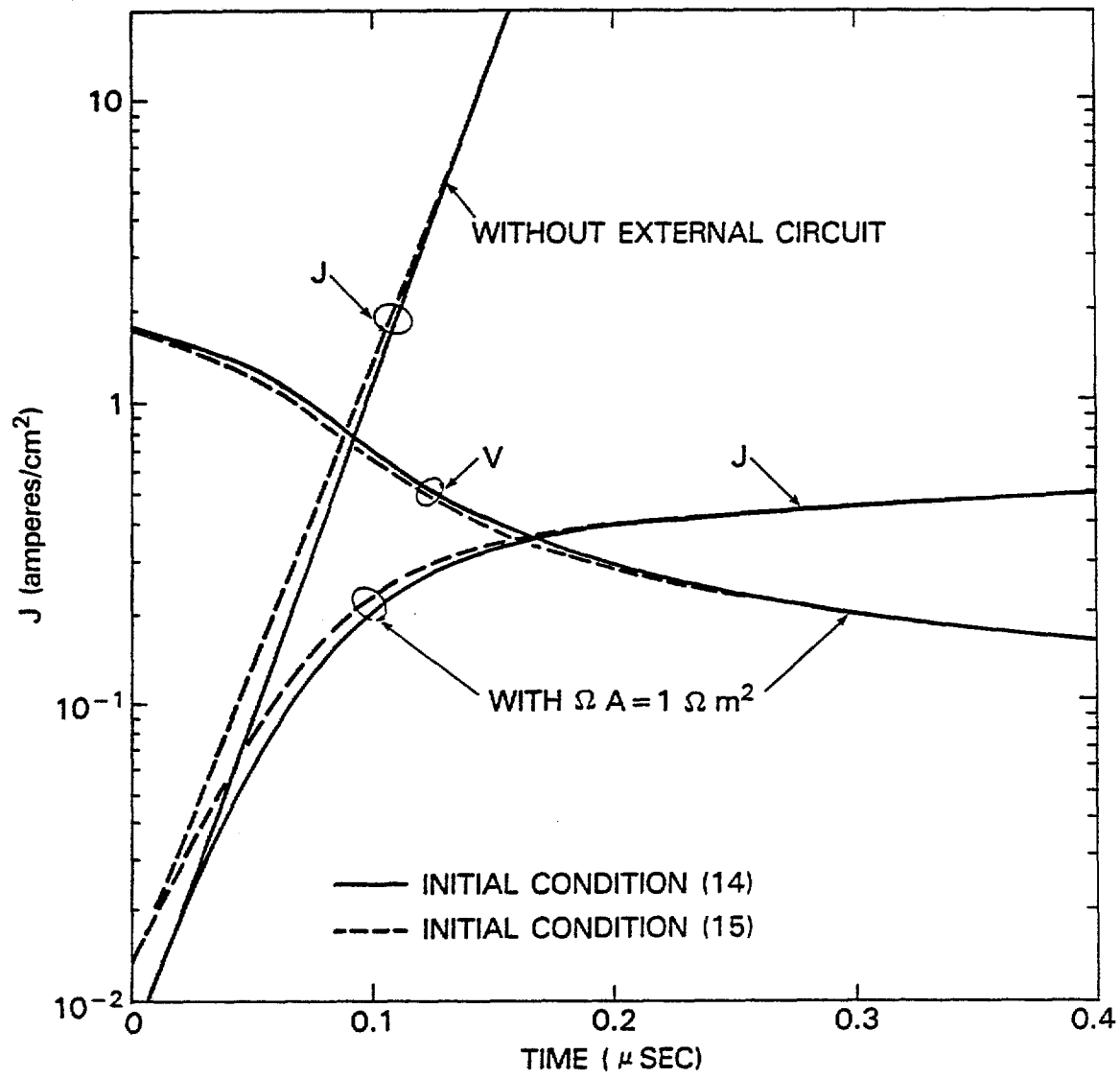


FIGURE 8. CALCULATED VOLTAGE AND CURRENT DENSITY VERSUS TIME IN THE CASES OF WITHOUT EXTERNAL CIRCUIT AND WITH  $\Omega A = 1 \Omega m^2$

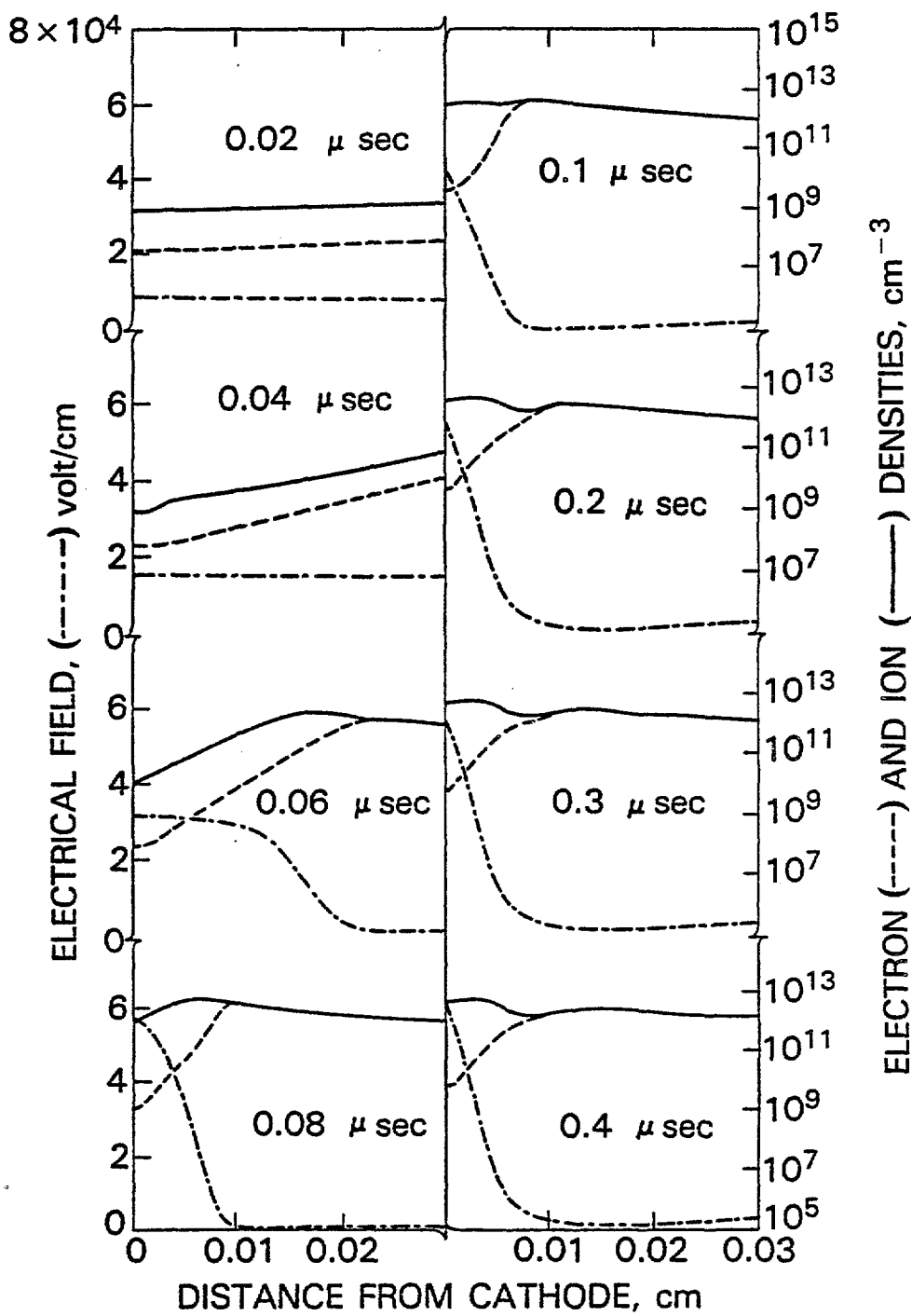


FIGURE 9. CALCULATIONS SIMILAR TO FIGURE 5 EXCEPT THAT THE EFFECT OF PHOTONS HAS BEEN CONSIDERED

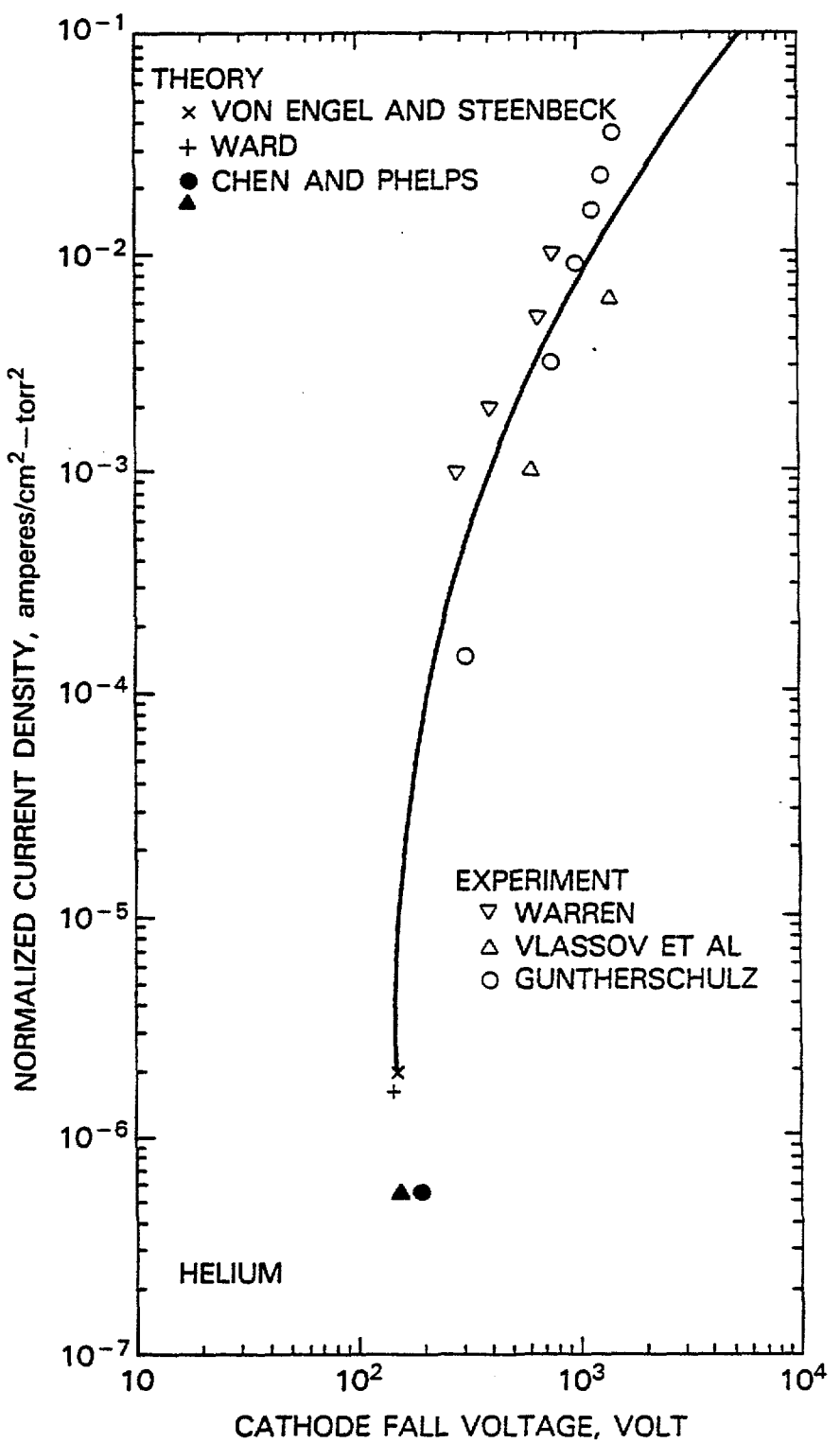


FIGURE 10. COMPARISON BETWEEN THEORY AND EXPERIMENT FOR THE STEADY STATE OF THE CATHODE FALL VOLTAGE VERSUS CURRENT DENSITY

## REFERENCES

1. J. W. Ward, *J. Appl. Phys.* 33, 2789 (1962). See also M. Nahemow, N. Wainfan and A. L. Ward, *Phys. Rev.* 137, A56 (1965).
2. L. E. Kline, *J. Appl. Phys.* 45, 2046 (1974); and 46 1567 (1975).
3. C. B. Mills, *J. Appl. Phys.* 45, 2112 (1974).
4. E. F. Jaeger, L. Oster and A. V. Phelps, *Phys. Fluids* 19, 819 (1976).
5. M. J. Druyvesteyn and F. M. Penning, *Rev. Mod. Phys.* 12, 87 (1940).
6. E. Segre, Editor, Experimental Nuclear Physics, Vol. 1 (John Wiley & Sons, Inc., 1960).
7. R. D. Richtmyer and K. W. Morton, Difference Methods for Initial Value Problems (Interscience, New York, 1967), H. Kriess, *Comm. Pure Appl. Math.* 17, 335 (1964).
8. I. Grabec, *Phys. Fluids* 17, 1834 (1974).
9. A. Guntherschulze and H. Schnitger, *Z. Physik* 77, 333 (1932); H. Mayer, *Phil. Mag.* 16, 594 (1933); A. Guntherschulze and F. Keller, *Z. Physik* 72, 143 (1931) and 79, 563 (1932).

10. A. V. Engel and M. Steenbeck, *Elektrische Gasentladungen*. Berlin: Springer 1932; R. Warren, *Phys. Rev.* 98, 1650 (1955).
11. E. McDaniel, *Collision Phenomena in Ionized Gases*, Wiley (1964).
12. A. V. Phelps, *Phys. Rev.* 117, 619 (1960).
13. W. P. Allis, *Revue de Phys. Appliquee* 10, 97 (1975).
14. J. J. Lowke and D. K. Davies, *J. Appl. Phys.* 48, 12 (1977). For the conditions of the present calculation, the formulas of this reference give an energy relaxation distance,  $\lambda_\epsilon$ , of  $\lambda_\epsilon = D/\mu E$ .
15. A. Guntherschulze, *Z. Physik* 49, 358, 473 (1928) and 59, 433 (1930); A. Guntherschulze and F. Keller, *Z. Physik* 71, 246 (1931) and 75, 105 (1932).
16. A. Guntherschulze, *Z. Physik* 59, 433 (1930).
17. J. D. Cobine, Gaseous Conductors (Dover, New York, 1958).

18. The calculated rate of heat input near the center of the cathode fall using the results shown in Fig. 4 is  $1 \text{ mW/cm}^3$  or  $2.3 \times 10^5 \text{ eV/atom-sec}$ . This corresponds to a temperature rise of about 250 K in 100 nsec. A sound wave would travel through the cathode fall region in about 10 nsec. The expanding low density region produced by heating in the cathode fall region has been observed experimentally. For example, Crawford and Phelps (unpublished) have made interferometric observations of this region and Rogoff has calculated some of its properties.

#### ACKNOWLEDGEMENTS

The authors wish to thank Drs. E. Jaeger, J. Gary, P. Swarztrumer and R. Sweet for many helpful discussions.

This work was supported in part by the Advanced Research Projects Agency and was monitored by the Office of Naval Research under Contract N00014-76-C-0123. Acknowledgement is made to the National Center for Atmospheric Research, which is sponsored by the National Science Foundation, for much of the computer time used in this research.

The paper is made possible by the Independent Research Fund at the Naval Surface Weapons Center.

## APPENDIX A

### STABILIZATION OF FINITE DIFFERENCE SCHEME BY MEANS OF A DIFFUSION TERM

First consider the unstable difference scheme for the hyperbolic equation

$$U_t + cU_x = 0$$

$$U_j^{n+1} = U_j^n - \frac{\lambda}{2} (U_{j+1}^n - U_{j-1}^n) \quad (A1)$$

where  $c$  is a constant and  $\lambda = c\Delta t/\Delta x$ .

The Lax-Wendroff scheme for the same equation is

$$U_j^{n+1} = U_j^n - \frac{\lambda}{2} (U_{j+1}^n - U_{j-1}^n) + \frac{\lambda^2}{2} (U_{j+1}^n - 2U_j^n + U_{j-1}^n) . \quad (A2)$$

It is stable provided  $|\lambda| < 1$ . We could regard this scheme as an obvious difference approximation to the equation  $U_t + cU_x = \epsilon U_{xx}$  where  $\epsilon = \lambda^2 \Delta x^2 / 2\Delta t$ .

In the limit as the mesh spacing approaches zero, our differential equation becomes  $U_t + cU_x = 0$ . Therefore we have added a diffusion type term in (A2) to an unstable scheme (A1) and thereby stabilized the scheme. Also, we might expect the solution of the difference scheme to converge to the solution of the hyperbolic equation.

Second, let us consider the Taylor series

$$\begin{aligned} U_j^{n+1} &\equiv U(x_j, t_n + \Delta t) \\ &= U(x_j, t_n) + \Delta t U_t(x_j, t_n) + \frac{\Delta t^2}{2} U_{tt}(x_j, t_n) + O(\Delta t^3) . \end{aligned} \quad (A3)$$

For the hyperbolic equation  $U_t = -cU_x$  we have  $U_{tt} = c^2 U_{xx}$ , thus (A3) becomes

$$U_j^{n+1} = U_j^n - c\Delta t U_x + \frac{c^2 \Delta t^2}{2} U_{xx} + O(\Delta t^3) . \quad (A4)$$

It is clear that we even improved the accuracy from  $O(\Delta t)$  to  $O(\Delta t^2)$  which gives from (A1) to (A2). This improved accuracy comes from the Taylor series expansion which produced the stable difference scheme.

The diffusion term regarded as a filter, the removal of energy in the high frequency modes can be done to pass low frequencies and block high frequencies. If we consider the equation

$$U_t + cU_x = aU_{xx} .$$

Using a Fourier series the solution is

$$U(x,t) = \sum_{k=-\infty}^{\infty} a_k e^{-a\pi^2 k^2 t} e^{i\pi k(x-ct)} .$$

If the term  $a\pi^2 k^2 t$  is quite small, then the solution approximates that of the hyperbolic equation  $U_t + cU_x = 0$ , namely

$$U(x,t) = \sum_{k=-\infty}^{\infty} a_k e^{i\pi k(x-ct)} .$$